

Solvent- and Temperature-Dependent Conformational Changes between Hückel Antiaromatic and Möbius Aromatic Species in *meso*-Trifluoromethyl Substituted [28]Hexaphyrins

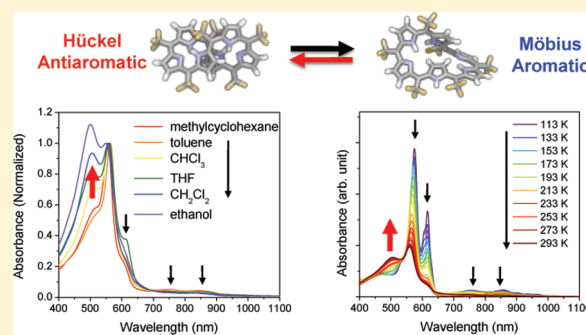
Min-Chul Yoon,[†] Pyosang Kim,[†] Hyejin Yoo,[†] Soji Shimizu,[‡] Taro Koide,[‡] Sumito Tokaji,[‡] Shohei Saito,[‡] Atsuhiro Osuka,^{*,‡} and Dongho Kim^{*,†}

[†]Spectroscopy Laboratory for Functional π -Electronic Systems and Department of Chemistry, Yonsei University, Seoul 120-749, Korea

[‡]Department of Chemistry, Graduate School of Science, Kyoto University, Sakyo-ku, Kyoto 606-8502, Japan

Supporting Information

ABSTRACT: We investigated the photophysical properties of figure-eight-like *meso*-hexakis(trifluoromethyl) [26]- and [28]hexaphyrins (1.1.1.1.1) denoted as TFM26H and TFM28H, respectively, using steady-state and time-resolved spectroscopy along with theoretical calculations to explore their electronic and magnetic natures depending on their molecular aromaticity. TFM26H exhibited a well-resolved absorption feature and intense fluorescence, both of which were neither solvent- nor temperature-dependent. These optical properties were in agreement with its Hückel's [$4n + 2$] aromaticity as observed in typical aromatic porphyrinoids. The S_1 -state lifetime of ~ 50 ps for TFM26H in solution was shorter than those in planar aromatic hexaphyrins (>100 ps) presumably due to nonplanar figure-eight geometry of TFM26H. However, TFM28H exhibited remarkable changes in solvent- and temperature-dependent absorption spectra as well as excited-state lifetimes indicating that a dynamic equilibrium occurs between the two conformational species. With the help of quantum mechanical geometry optimization and vertical excitation energy calculations, we found that the figure-eight double-sided conformer observed in the solid-state and single-sided distorted one could be the best candidates for the two conformers, which should be Hückel antiaromatic and Möbius aromatic species, respectively, based on their optical characteristics, molecular orbital structures, and excited-state lifetimes. Conformational dynamics between these two conformers of TFM28H was scrutinized in detail by temperature-dependent ^1H NMR spectra in various solvents, which showed that the conformational equilibrium was quite sensitive to solvents and that a conformational change faster than the NMR time-scale occurs even at 173 K.



INTRODUCTION

Molecular aromaticity in cyclic polyenes has been one of the most important concepts in chemistry over the last few decades.¹ Hückel's [$4n + 2$] and [$4n$] rules are convenient to predict the aromatic and antiaromatic nature of molecules, respectively, by directly counting the number of π -electrons participating in π -conjugation pathways in planar annulene systems.^{2,3} Recently, other types of aromatic compounds extending to nonplanar systems have been synthesized such as Möbius molecules, figure-eight Hückel aromatic molecules, and so on.^{4–11} Despite their importance in chemistry, the photophysical properties depending on the Hückel/Möbius aromaticity have rarely been investigated, whereas theoretical approaches have been widely used mainly because Hückel antiaromatic as well as Möbius aromatic compounds are not easily formed in common hydrocarbon annulene systems.⁷

Conventional Möbius topological molecules have a π twist around the ring, while classical Hückel systems are represented by a single planar ring without any twists. Möbius aromaticity was

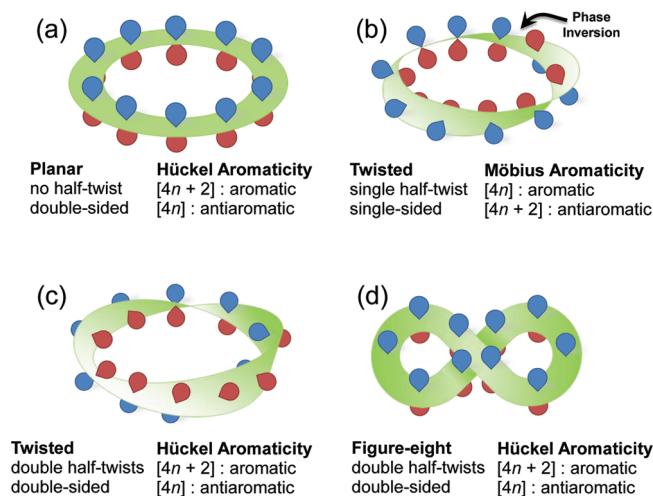
coined for aromatic characters acquired by the molecules having [$4n$] π -electrons with Möbius topology as predicted by Heilbronner.^{9,12} Nonplanar three-dimensional π -conjugated annulene systems can be generally classified into Hückel or Möbius systems based on their structural topologies using mathematical approaches with a coiled ribbon model proposed by Rzepa and co-workers.⁵ In their extended definition, three-dimensionally multiply-twisted molecules with an even integer for the linking number (L_k) are aromatic when they have [$4n + 2$] π -electrons, which satisfy Hückel's [$4n + 2$] rule (Hückel aromaticity). However, twisted molecules with an odd integer for the L_k value are aromatic when they have [$4n$] π -electrons (Möbius aromaticity). The linking number (L_k) consists of the twisting number (T_w) and writhing number (W_r) with the relationship $L_k = T_w + W_r$, where the three parameters have units of π .

Received: August 12, 2011

Revised: October 10, 2011

Published: October 27, 2011

Scheme 1. Schematic Illustration of the Conjugated π -Electronic Systems Whose Topological and Aromatic Properties Related to the Number of π -Electrons (n) Are Specified^a

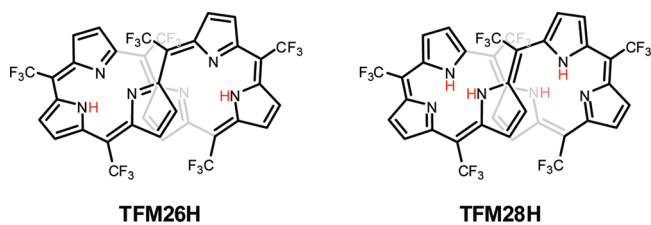


^a On the basis of the generalized Hückel rule, c and d topologically belong to the double-twist Möbius molecules.⁵

T_w is the sum of the local relative twists of the atoms in the ring indicating an overlap between the adjacent atomic p -orbitals. However, W_r is a nonlocal property representing the strain of the molecular loops. Besides the difficulty of the numerical calculations for T_w and W_r , it is important that the molecular aromaticity is governed only by the linking number, L_k . According to this generalized Hückel rule, four representative schematic topologies illustrating molecular aromaticity in relatively small annulenes are shown in Scheme 1.

Expanded porphyrins, which have more than five pyrroles in their macrocycles, are ideal candidates to study the molecular aromaticity because of their unique chemical and optical properties with enhanced stability.^{13,14} More importantly, the two-electron redox reactions of the expanded porphyrins are generally facile, allowing for the formation of neutral $[4n+2]$ and $[4n]$ π -electronic species from the same molecular framework as compared to typical annulenes.¹⁵ Among these expanded porphyrins, the authors have especially focused on hexapyrrolic systems due to their structural stability, higher molecular symmetry, and versatile metalation behaviors.^{16–20} Recently, the photophysical properties of various *meso*-aryl substituted [26]- and [28]hexaphyrins were comparatively investigated in relationship to their molecular aromaticity such as planar Hückel antiaromatic^{16,17} and distorted Möbius aromatic [28]hexaphyrins.^{21–23} These works have shown that Hückel antiaromatic hexaphyrins have quite distinctive photophysical features such as broad and featureless absorption spectra with an optically dark S_1 -state expected to exist in the NIR region, a lack of fluorescence, and a short S_1 -state lifetime (10–30 ps), while aromatic hexaphyrins exhibit similar optical properties to each other (strong fluorescence with a long S_1 -state lifetime of >100 ps) whether the molecules complied with Hückel or Möbius aromaticity.^{16,24} The molecular switching behavior between aromatic and antiaromatic conformers was also discovered by means of temperature-dependent ^1H NMR spectroscopy in another $[4n]$ π -electronic system, di-*p*-benzyl [28]hexaphyrins, by Latos-Grażyński and co-workers.^{25,26} In all cases, [28]hexaphyrins tend to avoid Hückel antiaromatic

Chart 1. Molecular Structures of TFM26H and TFM28H Based on X-Ray Crystallographic Data



conformations and prefer distorted Möbius aromatic conformers to reduce their internal energies.

meso-Trifluoromethyl (TFM) substituted expanded porphyrins have been synthesized in a straightforward manner and isolated and characterized up to decaphyrin.²⁷ Among these, *meso*-TFM substituted [26]- and [28]hexaphyrins denoted as TFM26H and TFM28H, respectively (Chart 1), are interesting in that both macrocycles take similar figure-eight structures in the solid-state despite the difference in the number of π -electrons. Since these two conformations have double half-twists with $L_k = 2$, it is thought that TFM26H and TFM28H could be simply assigned as Hückel aromatic and antiaromatic species, respectively (Scheme 1d). However, it turned out that both the experimental²⁷ and theoretical investigations were difficult to reconcile with this simple assignment.^{28–30} The ^1H NMR spectrum of TFM26H showed six peaks ($\delta = 7.88, 7.67, 7.54, 7.38, 6.33$, and 5.99 ppm) and a single peak (11.11 ppm) due to the β -CH and NH protons, respectively, in CDCl_3 at room temperature. These data indicate there was no strong diatropic ring current for TFM26H making it tempting to assign TFM26H as a nonaromatic species.²⁷ However, theoretical approaches by the Rzepa group^{28,29} and Fliegl et al.³⁰ indicated that TFM26H should certainly be aromatic. In addition, they proposed the possibility of a NH tautomer for TFM26H, which resulted in a slightly reduced diatropic ring current based on a ^1H NMR simulation. However, the ^1H NMR spectrum of TFM28H in CD_2Cl_2 at room temperature showed two peaks due to the NH protons at $\delta = 14.95$ and 12.35 ppm and rather broad peaks due to the β -CH protons between $\delta = 7.37$ and 6.88 ppm, which became split into six peaks at -80°C .²⁷ This indicates that TFM28H has a C_2 symmetry and is slightly antiaromatic at low temperatures, but the broad spectrum suggests a conformational equilibrium at room temperature, which has not yet been revealed. The Rzepa group and Fliegl et al. assigned TFM28H to be antiaromatic based on the X-ray and the quantum mechanically optimized figure-eight structures.^{28–30} Despite their insightful analyses, however, the simulated ^1H NMR peaks were slightly more deshielded by 3–4 ppm from the NH protons of TFM28H, which could not explain the observed unusual absorption spectrum of TFM28H.

In this work, a comparative study on the photophysical properties between TFM26H and TFM28H in solution was done. In this study, a particular focus was placed on the absorption spectra of TFM28H, which showed some differences from those of typical antiaromatic hexaphyrins. On the basis of the obtained results, this study will show that TFM28H exists as a dynamic equilibrium of aromatic and antiaromatic conformers and that the selective optical probing of a particular one among various conformational isomers with different aromatic characteristics is possible. Temperature- and solvent-dependent conformational dynamics will be

addressed with ground-state potential energy surfaces based on the ^1H NMR spectroscopic results. Furthermore, the most plausible structures in aromatic and antiaromatic congeners in solution will be proposed, which provides important insight into the relationship between molecular structure and aromaticity.

■ EXPERIMENTAL SECTION

Sample Preparation. Details in synthesis, characterization, and X-ray crystallographic analysis of **TFM26H** and **TFM28H** were described elsewhere.²⁷ All reagents and solvents were of commercial reagent grade and were used without further purification.

Temperature-Dependent NMR. All temperature-dependent ^1H NMR spectra were recorded on a JEOL ECA-600 spectrometer (600.17 MHz for ^1H), and chemical shifts were reported as the delta scale in ppm relative to residual solvent in CDCl_3 (^1H NMR: $\delta = 7.26$ ppm), THF- d_8 (^1H NMR: $\delta = 1.72$ ppm) or 1,1,2,2-tetrachloroethane- d_2 (^1H NMR: $\delta = 5.98$).

Steady-State Absorption and Fluorescence. UV-vis/NIR absorption spectra were recorded on a commercial absorption spectrometer (Varian, Cary5000). The NIR fluorescence was measured using a monochromator (Acton Research Co., SP2150) with a focal length of 15 cm attached with a TE-cooled near-infrared (NIR) photomultiplier (Hamamatsu, H9170-75) and a lock-in amplifier (EG&G, DSP-7265) combined with a mechanical chopper after laser excitation at 532 nm from a continuous wave (CW) Nd:YLF laser (Coherent, Verdi V). A quartz cell with an optical path length of 10 mm was used for all steady-state measurements. For temperature-dependent absorption measurement, a temperature-controlled liquid nitrogen cryostat (Oxford Instruments, Optistat DN) was used. Temperatures were maintained to within ± 0.05 K and allowed to equilibrate for at least 30 min in each scan.

Femtosecond Transient Absorption. The femtosecond time-resolved transient absorption (TA) spectrometer consisted of a homemade noncollinearly phase-matched optical parametric amplifier (NOPA) pumped by a Ti:sapphire regenerative amplifier system (Quantronix, Integra-C) operating at 1 kHz repetition rate and an optical detection system. The generated visible NOPA pulses had a pulse width of ~ 100 fs and an average power of 1 mW in the range 480–700 nm, which were used as pump pulses. White light continuum (WLC) probe pulses were generated using a sapphire window (2 mm of thickness) by focusing a small portion of the fundamental 800 nm pulses, which was picked off by a beam splitter before entering the NOPA. The time delay between pump and probe beams was carefully controlled by making the pump beam travel along a variable optical delay (Newport, ILS250). Intensities of the spectrally dispersed WLC probe pulses are monitored by a miniature CCD-spectrograph (OceanOptics, USB2000+). To obtain the time-resolved transient absorption difference signal (ΔA) at a specific time, the pump pulses were chopped at 25 Hz, and absorption spectra intensities were saved alternately with or without pump pulse. Typically, 6000 pulses excite samples to obtain the TA spectra at a particular delay time. The polarization angle between the pump and probe beam was set at the magic angle (54.7°) using a Glan-laser polarizer with a half-wave retarder in order to prevent polarization-dependent signals. Cross-correlation fwhm in pump–probe experiments was less than 200 fs, and the chirp of WLC probe pulses was measured to be 800 fs in the 450–850 nm region. To minimize the chirp, all reflection optics

in the probe beam path and 2 mm path length of a quartz cell were used. After fluorescence and TA experiments, we carefully checked absorption spectra of all compounds to avoid artifact from degradation and photo-oxidation of samples. The HPLC grade solvents (Aldrich) were used in all steady-state and time-resolved spectroscopic studies. Decay associated spectra were obtained by global fitting analysis of the measured time-resolved TA data using a commercial software (Surface Explorer Pro, Ultrafast Systems) with chirp compensation and singular value deposition method.

Computational Methods. Quantum mechanical calculations were performed by the Gaussian03 program suite installed on a supercomputer (IMB p690, KISTI).³¹ Geometry optimizations were carried out by the density functional theory (DFT) method with the Becke's three-parameter hybrid exchange functional and the Lee–Yang–Parr correlation functional (B3LYP),^{32,33} employing a basis set containing 6-31G(d) for all atoms.³⁴ The X-ray crystallographic structures were used as initial geometries for geometry optimization.²⁷ After geometry optimization procedures, frequency calculations were done at the same levels to check whether the optimized geometries lie on the local minima of potential energy surface. It was found that there was no imaginary vibrational frequency for all the optimized structures. The simulated ^1H NMR data and nucleus-independent chemical shift (NICS) values were calculated by the gauge-including atomic orbital (GIAO) method^{35,36} at the B3LYP/6-31G(d,p) level based on optimized geometries without any modification for all molecules. NICS values evaluated on three nonweighted centroids due to the three-dimensionally nonplanar structures. In order to calculate the chemical shifts of the protons, we used the averaged ^1H NMR chemical shift value of 31.75 ppm calculated at the B3LYP/6-31G(d,p) level for tetramethylsilane (TMS, optimized at B3LYP/6-31G(d,p)) as an internal reference. To simulate the ground-state absorption spectra, we used time-dependent (TD) DFT calculations³⁷ with the same functional and basis set as was used in the geometry optimization. All computational analyses were carried out including all the peripheral substituents (six trifluoromethyl groups) since substituent effects should not be negligible in porphyrin and expanded porphyrin systems.¹⁴

■ RESULTS AND DISCUSSION

Steady-State Absorption and Fluorescence Spectra. The steady-state absorption and fluorescence spectra of **TFM26H** and **TFM28H** were recorded in toluene and CH_2Cl_2 at room temperature (Figure 1). The overall spectral characteristics of both the absorption and fluorescence spectra of **TFM26H** and **TFM28H** were quite similar to those of *meso*-pentafluorophenyl substituted [26]- and [28]hexaphyrins.^{19,21} The absorption spectrum of **TFM26H** in toluene exhibited an intense Soret-like (B-like) band appearing at 583 nm and four weak Q-like bands with vibronic structures at 749, 833, 917, and 1061 nm. A similar spectrum was observed in CH_2Cl_2 , indicating that **TFM26H** took similar conformations in both solvents. In addition, the well-resolved absorption and relatively strong NIR-fluorescence spectrum of **TFM26H** resembled those of typical aromatic porphyrinoids^{14,15} and indicated that **TFM26H** seemed to have a strong aromatic character in solution at room temperature. However, **TFM28H** showed a remarkable difference in its absorption spectra for the two solvents (Figure 1). The steady-state spectroscopic data of **TFM28H** in toluene had similar

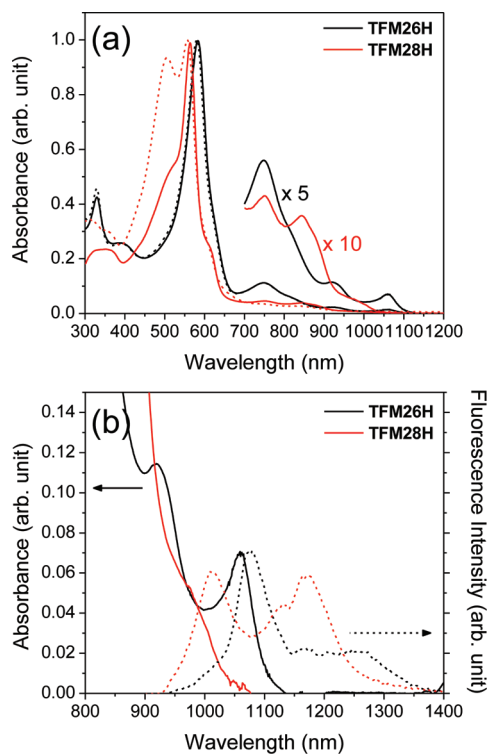


Figure 1. (a) Absorption spectra of TFM26H (black line) and TFM28H (red line) in toluene (solid line) and CH_2Cl_2 (dashed line). (b) NIR fluorescence spectra of TFM26H (black dashed line) and TFM28H (red dashed line) with photoexcitation at 532 nm in toluene. Absorption and emission spectra are normalized to the highest absorption and the lowest absorption bands, respectively. The absorption bands in the 700–1200 nm region are magnified for the clarity.

features to that of *meso*-pentafluorophenyl [28]hexaphyrins¹⁹ such as an intense B-like band at 563 nm, four weak Q-like bands at 750, 842, 883, and 959 nm, and a relatively strong and well-resolved NIR-fluorescence spectrum except for a weak absorption band appearing around 500 nm. It should be noted that this characteristic band around 500 nm was considerably larger in CH_2Cl_2 than in toluene, inferring that other conformational species might exist and its contribution might be larger in CH_2Cl_2 . Compared with those of vinylene-bridged [26]- and [28]hexaphyrins,¹⁶ the three times smaller extinction coefficients and broad absorption spectra for both TFM26H and TFM28H suggest that there was increased flexibility in the figure-eight structures (Figure S1 in the Supporting Information).

Solvent- and Temperature-Dependent Absorption Spectra. To gain an insight into the existence of conformational isomers, the absorption spectra of TFM26H and TFM28H were measured in various solvents at room temperature. Although the absorption spectra of TFM26H did not show any significant solvent-dependent changes (Figure S2 in the Supporting Information), those of TFM28H exhibited dramatic changes depending on the dielectric constants of the solvents as seen in Figure 2a. In the case of TFM28H, as the dielectric constant of the solvent increased going from methylcyclohexane ($\epsilon = 2.02$) to ethanol ($\epsilon = 25.3$), the relative intensity of the B-like band at ~ 500 nm gradually increased, while all the weaker bands at wavelengths longer than 600 nm decreased. On the basis of this result, the assumption can be made that at least two conformational

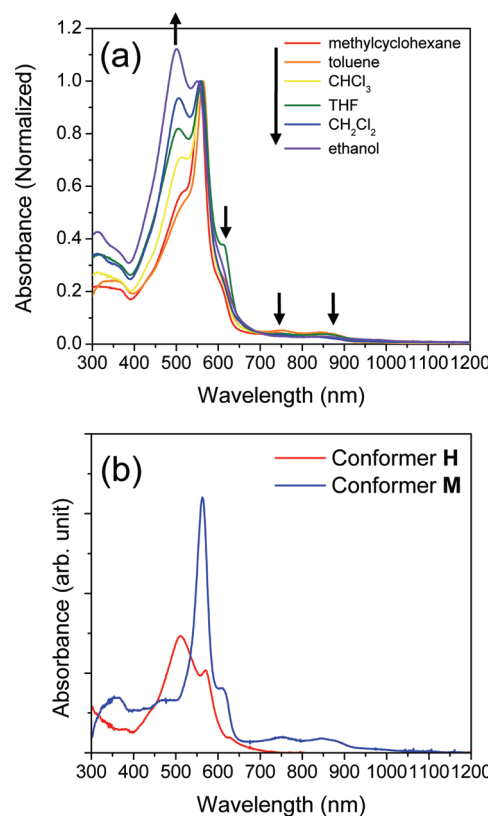


Figure 2. (a) Absorption spectra of TFM28H in various solvents, which are normalized to the intensity of the peak at 560 nm for comparison purposes. Vertical arrows indicate the direction of increasing dielectric constant of solvent. (b) Estimated absorption spectra of two conformers of TFM28H in solution retrieved from a.

isomers of TFM28H should exist in solution at room temperature, whereas there is only a single conformer of TFM26H in solution at room temperature.

In the case of TFM28H, the intrinsic absorption spectrum of each conformer can be obtained by subtracting the measured solvent-dependent absorption spectra because the peak shifts upon changing the solvent were very small (<5 nm) in the whole spectral region (Figure 2b). Hereafter, these two conformational isomers are denoted as conformers H and M of which the Soret-bands appeared at 500 and 560 nm, respectively. It is of interest that the overall spectral features of these two absorption spectra are much different from each other. Moreover, the absorption spectral shapes of conformers H and M resemble those of vinylene-bridged Hückel aromatic [26]- and antiaromatic [28]hexaphyrins, respectively (Figure S3 in the Supporting Information).¹⁶ On the basis of these spectral features, it can be postulated that conformers M and H correspond to aromatic and antiaromatic conformers, respectively. It is believed that the observed fluorescence of TFM28H in the NIR region mainly comes from conformer M because of its relatively strong absorption bands extending up to 1100 nm, which is in good agreement with the strong fluorescent behaviors of typical aromatic expanded porphyrins.¹⁴ Furthermore, since the equilibrium between the two conformers at room temperature was highly sensitive to the dielectric constant of the solvent, it is inferred that dipole-mediated solvation plays an important role in their equilibrium described by Onsager's model.³⁸

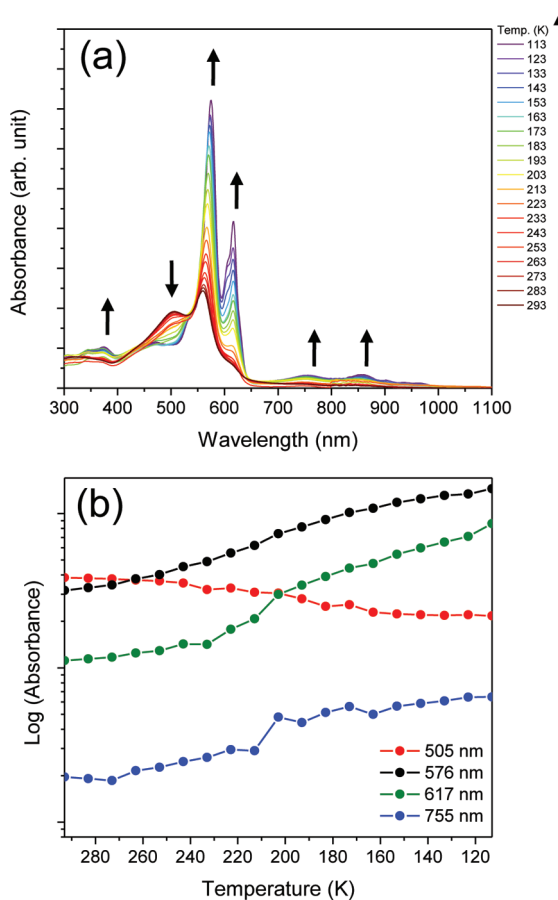


Figure 3. (a) Temperature-dependent absorption spectra and (b) logarithmic plot of absorbance change as a function of temperature at specific wavelengths of TFM28H in 2-MTHF. In a, arrows indicate the direction of decreasing temperature.

To examine the equilibrium conformational dynamics, the absorption spectra of TFM26H and TFM28H in 2-methyltetrahydrofuran (2-MTHF) were recorded in the temperature range of 113–293 K. In the case of TFM26H, as the temperature decreased, the intensities of all the bands gradually increased with a slight sharpening of the B-like bands presumably due to the enhanced molecular rigidity (Figure S4 in the Supporting Information). However, the temperature-dependent absorption spectra of TFM28H showed much different behaviors as shown in Figure 3. As the temperature decreased, the intensities of all the bands progressively increased similar to TFM26H, whereas the band around 500 nm corresponding to the absorption of conformer H diminished significantly. According to the solvent-dependent absorption spectra of TFM28H, the decreased and increased absorption bands upon lowering the temperature originated from conformers H and M, respectively. In other words, in the case of TFM28H, conformers H and M were the dominant species at high and low temperatures for their equilibrium conformational dynamics, respectively, inferring that conformer M should be more energetically stable in the solution phase. Similar behavior was also found in the case of meso-pentafluorophenyl [28]hexaphyrins,^{21,22} where a fast interconversion between Hückel antiaromatic and Möbius aromatic conformers and their dynamic equilibrium depending on the temperature were observed. Moreover, most of the meso-aryl

[28]hexaphyrins exist as Möbius aromatic conformers at room temperature indicating that most of the spectroscopic characteristics come from the Möbius aromatic conformer.^{21,22} In this work, therefore, the authors believe that TFM28H with a [4n] π -electronic circuit has two conformational isomers of Hückel antiaromatic and Möbius aromatic conformers in solution, which correspond to the conformers H and M, respectively.

Quantum Mechanical Calculations. In order to determine the structures of the conformational isomers (a single aromatic conformer for TFM26H and two (aromatic and antiaromatic) conformers for TFM28H), quantum mechanical geometry optimization was done at the B3LYP/6-31G(d) level. Three sets of optimized structures were obtained with figure-eight, partially distorted and saddle-like relatively planar orientations for both compounds, respectively (Figure S5 and Table S2 in the Supporting Information). These various energetically stable structures were feasible mainly due to the small steric hindrance of the meso-trifluoromethyl substituents. In the case of TFM26H, the figure-eight optimized geometry being similar to the X-ray crystallographic structure was calculated to be the most stable conformer with the energy of 5000 cm^{-1} , which was lower compared to the others. Hence, it may be concluded that the single species appearing in all spectroscopic measurements of TFM26H corresponds to this figure-eight conformer, which is regarded as a Hückel aromatic molecule (Scheme 1d). However, the three optimized conformers for TFM28H did not have any significant differences in energy. However, the saddle-like conformer with the highest energy can be neglected as a possible conformation because only two conformers were found in solution. Moreover, the orientation of the partially distorted conformation is quite similar to the single-sided Möbius structure seen in meso-pentafluorophenyl substituted [28]hexaphyrins,^{21,22} supporting that one of the two conformers has an aromatic nature as inferred from the spectroscopic data. In agreement with the experimental findings, while the two conformers are predicted to have comparable energies, conformer H (Hückel antiaromatic) was more stable by 14.7 kJ mol^{-1} compared to conformer M (Möbius aromatic). The energy ordering has no quantitative significance since the calculations were done without surrounding solvent molecules.²⁴ Accordingly, it can be concluded that Möbius aromatic and Hückel antiaromatic conformers are good candidates for the two species of TFM28H observed in solution as shown in Figure 4.

In addition, although typical planar porphyrinoids exhibit negligible dipole moments in ground electronic states, the calculated dipole moments of the three optimized structures exceeded 1 D, which are mainly due to their nonplanar geometries (Figure S6 in the Supporting Information). It should be noted that the orientations of the dipole moments of the two conformers in TFM28H are very different despite similar strengths, which might be the origin of the influence of the large solvent dependence on the absorption spectra.

The aromatic characteristics of the three conformational candidates were examined using two general indices for aromaticity: the harmonic oscillator model of aromaticity (HOMA) along [26] and [28] π -conjugation pathways¹ and the nucleus-independent chemical shift (NICS) values at the nonweighted center of the ring (Figures S7 and S8 in the Supporting Information).^{39,40} HOMA values close to unity (0.78 and 0.76) and large negative NICS values (-11.5 and -12.4 ppm) indicated the strong aromatic natures of TFM26H and conformer M of TFM28H, respectively, which is in good agreement with

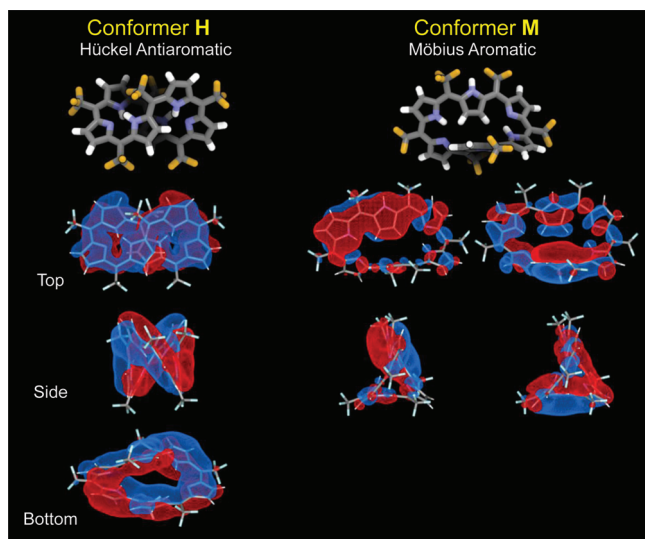


Figure 4. Optimized structures and molecular orbital densities of the lowest π -MOs for conformers **H** (left side with 161th MO) and **M** (right side with 159th and 162th MOs).

other theoretical studies.^{29,30} However, conformer **H** of **TFM28H** had a positive NICS value (5.6 ppm) with a relatively small HOMA value of 0.55 indicating its antiaromatic nature. All the data are consistent with Herges' investigation on the relationship between the HOMA and NICS values.⁷ These features indicate that π -electrons are well-delocalized in all systems. On the basis of the MO analysis, the lowest π -MOs of conformers **H** and **M** also support the Hückel antiaromatic and Möbius aromatic nature of the conformers because there is no node and one node, respectively (Figure 4).¹⁴

Femtosecond Transient Absorption and Electronic Structures. To elucidate the excited state dynamics, the femtosecond transient absorption (TA) spectra of **TFM26H** and **TFM28H** were measured. The TA spectra of **TFM26H** in toluene with photoexcitation of the most intense B-like band at 580 nm showed a similar trend compared to those of typical aromatic planar expanded porphyrins (Figure S9 in the Supporting Information).¹⁴ Strong negative signals by ground state bleaching recovery (GSB) at the 580 nm region with broad positive signals due to excited state absorption (ESA) were observed in which the whole spectral shapes did not change within a temporal window of 1 ns. The least-squares fitting method with a convoluted function of multi-exponential decay with a Gaussian instrument response function was used to analyze the decay profiles probed at two representative wavelengths including the GSB and ESA signals (570 and 660 nm, respectively), which yielded two time constants of 1 and 55 ps, respectively (Figure S9 in the Supporting Information). The former one seems to arise from the internal conversion of a B-like state to a Q-like state as well as vibrational relaxation processes. The latter one with the large amplitude should correspond to the lifetime of the lowest singlet excited state (S_1). In addition, the TA spectra and temporal profiles of **TFM26H** in CH_2Cl_2 yielded no significant changes compared with those in toluene, which yielded an S_1 -state lifetime of 53 ps (Figure S9 in the Supporting Information). The S_1 -state lifetimes of **TFM26H** were shorter than those of *meso*-pentafluorophenyl (\sim 100 ps) and vinylene-bridged (\sim 280 ps) [26]hexaphyrins^{16,21} indicating that the S_1 -state lifetimes become longer in increasing order of molecular rigidity.

In the case of **TFM28H**, the TA spectra with photoexcitation at two B-like bands centered at 500 and 560 nm for selective excitation of conformers **H** and **M** were measured, respectively (Figure 5). It was noted that the rigorous selective excitation of a single conformer was impossible due to an appreciable spectral overlap of both conformers in the B-like band region (see Figure 2b). Nevertheless, the excitation wavelength-dependent spectral changes were clearly seen in their TA spectra in which the two sets of TA spectra for **TFM28H** in toluene exhibited distinctly different behaviors. In the TA spectra obtained by photoexcitation at 500 nm, two main GSB signals at 500 and 560 nm were observed (Figure 5a). In addition, the GSB and ESA signals at 507 and 650 nm, respectively, rapidly decayed within a few ps, which was at least 20 times shorter than the decay time of the GSB band at 565 nm (Figure 5e). The decay associated spectra obtained with the help of global analysis yielded four transient species in **TFM28H** with decay time constants of 1, 10, 255, and >5000 ps (Figure 5c). It was noted that similar spectral shapes and temporal evolution of the TA spectra with time constants of 1 and 10 ps were observed as compared with those in the planar Hückel antiaromatic vinylene-bridged [28]hexaphyrins (0.53 and 8.6 ps in toluene),¹⁶ which indicates that these TA spectra mainly originated from the Hückel antiaromatic conformer. Furthermore, because the ground state absorption spectrum of conformer **H** of **TFM28H** supported by the results of the solvent- and temperature-dependent experiments is well matched with these TA spectra, conformer **H** should be the Hückel antiaromatic species. On the contrary, the transients with decay time constants of 255 ps and >5 ns can be ascribed to the S_1 - and T_1 -state lifetimes of conformer **M** of **TFM28H**, respectively, since the spectral shapes as well as the time constants were similar to those of the distorted Möbius aromatic hexaphyrins, the *meso*-aryl [28]hexaphyrins.²¹ When the excitation wavelength was tuned to the B-like band for conformer **M** of **TFM28H** at 560 nm, some spectral differences were revealed in the TA spectra (Figure 5b,d,f). While the decay parameters as well as the decay associated TA spectral shapes were similar to each other, the magnitudes of the GSB signals of conformers **H** (500 nm) and **M** (560 nm), especially in their decay associated spectra with time constants of \sim 1 and 250 ps, respectively, were quite different (Figure 5c,d). These results clearly show that the excited state population of conformer **H** was larger than that of conformer **M** by the selective excitation of conformer **H** at 500 nm and vice versa. These excitation wavelength-dependent excited population changes also strongly support the existence of two conformers in **TFM28H** and their aromaticity. TA measurements of **TFM28H** in CH_2Cl_2 also provided similar excitation wavelength dependency to those in toluene (Figure S10 in the Supporting Information). When compared to toluene, the relative intensities of the TA spectra for conformer **H** was much larger than those of conformer **M** in CH_2Cl_2 , which is in agreement with the steady-state absorption data showing a more intense absorption for conformer **H** (Figure 1).

The energy relaxation dynamics observed in the TA measurements can be explained by the help of molecular orbital and vertical excitation energy calculations using the optimized structures. The calculated vertical excitation energy spectrum of **TFM26H** is in agreement with the absorption spectrum resulting from the configuration interactions between four frontier MOs described by Gouterman's model,⁴¹ indicating that the figure-eight [26]hexaphyrin is also a Hückel aromatic species (Figures S11 and S12 in the Supporting Information).^{16,24} In a similar manner,

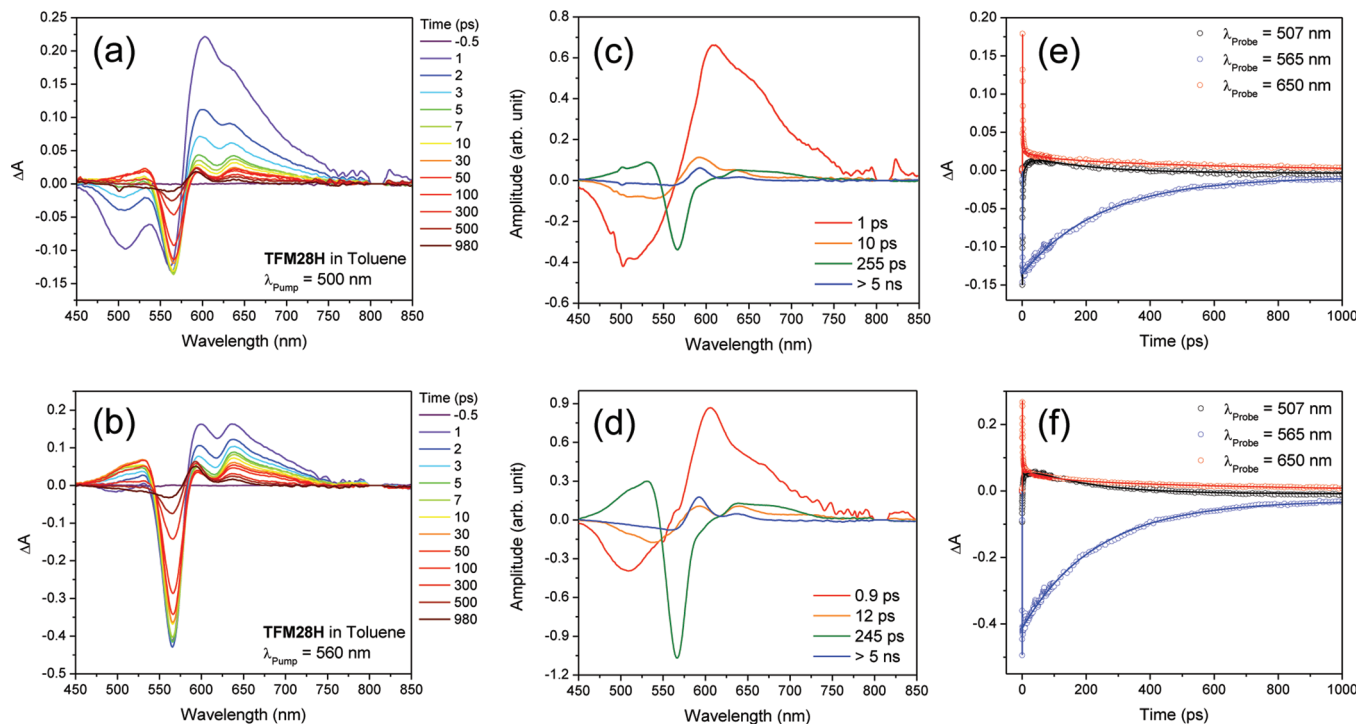


Figure 5. Transient absorption spectra (left), decay associated spectra (middle), and temporal profiles (right) of TFM28H in toluene with photoexcitation at 500 (a, c, and e) and 560 nm (b, d, and f).

the whole spectral features of TFM28H can be explained by the summation of the two vertical excitation energy spectra for the two possible conformers, the figure-eight and distorted one. For the distorted conformer, the simulated absorption spectrum was similar to the measured one of conformer M (Figure S12b in the Supporting Information). These spectral shapes can also be observed in $[4n]\pi$ -electronic [28]hexaphyrins with a Möbius aromatic nature.^{21,22} On the contrary, the calculated five optical transitions (1705, 667, 647, 502, and 469 nm) from the configuration interactions involving six frontier MOs were observed in the TD-DFT calculations for the figure-eight conformation of TFM28H, which was similar to the observed absorption peaks for conformer H (Figure 2b). The lowest singlet state at 1705 nm came from a direct HOMO–LUMO transition with an extremely low oscillator strength of 0.0002, corresponding to a one-photon optically forbidden transition, which is a unique feature for typical antiaromatic porphyrins based on the Hückel topology (see Figure S12 and Table S3 in the Supporting Information).^{16,17,24,42} Because this state can act as a ladder state in excited energy relaxation processes, the observed short excited-state lifetime (~ 10 ps) for the antiaromatic conformer H in TFM28H might be due to the accelerated internal conversion rate to the ground electronic state as expected by the energy-gap law (Figure S13 in the Supporting Information).

Solvent- and Temperature-Dependent ^1H NMR Spectra. ^1H NMR spectroscopy is one of the best ways to investigate the molecular aromaticity.^{25,43} The temperature-dependent ^1H NMR spectra were recorded in various solvents to gain deep insight into the equilibrium dynamics and structural information on the two conformers in conjunction with their aromaticities. Figure 6 shows the ^1H NMR spectra of TFM28H recorded in the temperature range of 173–298 K in $\text{THF}-d_8$. Upon lowering the temperature from 298 to 173 K, the ^1H NMR spectra exhibited

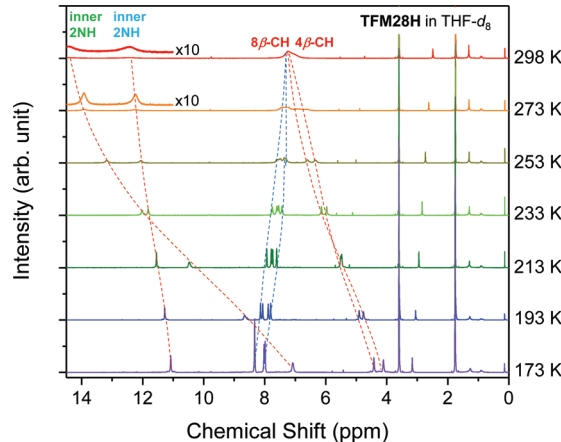


Figure 6. Temperature-dependent ^1H NMR spectra of TFM28H in $\text{THF}-d_8$.

dramatic changes as follows: (i) the most deshielded signal of the NH proton (14.43 ppm) was upfield shifted to 7.08 ppm, and interestingly, the peak positions for two NH protons crossed between 233 and 213 K; (ii) the congested signal due to the six β -CH protons observed at 7.22 ppm split into a set of slightly deshielded four peaks (7.98–8.33 ppm) and a set of shielded two peaks (4.11 and 4.42 ppm); and (iii) the intensities of all the signals increased. These spectral changes can be interpreted in terms of suppressed conformational dynamics at low temperatures; a rapidly interconverting conformational mixture became split into two sets of conformers. At high temperature (> 300 K), the simulated ^1H NMR spectrum exhibited a strong paratropic ring current, indicating that conformer H is antiaromatic.

However, the diatropic ring current becomes dominant at temperature lower than 150 K, indicating that conformer **M** should be aromatic. In contrast with the spectral changes in the ^1H NMR spectra of TFM28H, there was no significant temperature dependence in TFM26H (not shown), which is in agreement with the solvent- and temperature-dependent absorption measurements.

In order to analyze quantitatively the temperature-dependent ^1H NMR spectra of TFM28H, a thermodynamic model based on the van't Hoff equation was introduced.²⁴ Consider a reversible interconversion between two chemical species as follows:



where the species **H** and **M** represent conformers **H** and **M** in TFM28H. If the conformational interconversion rate between **H** and **M** is faster than the ^1H NMR time scale in the temperature range of 173–298 K, the observed ^1H NMR chemical shift values can be regarded as the weighted average of the chemical shifts for the two conformational isomers.^{44,45} Hence, the observed chemical shift $\delta^i(T)$ of proton *i* at given temperature *T* can be expressed by the following equation:

$$\delta^i(T) = x_{\text{H}}(T)\delta_{\text{H}}^i + x_{\text{M}}(T)\delta_{\text{M}}^i \quad (1)$$

where $x_{\text{H}}(T)$ and $x_{\text{M}}(T)$ are the mole fractions of conformers **H** and **M** at temperature *T*, and δ_{H}^i and δ_{M}^i are the chemical shifts of the *i*-th protons in conformers **H** and **M**, respectively. Furthermore, based on the van't Hoff equation, the equilibrium constant $K(T)$ for this reversible reaction can be written as

$$K(T) = \frac{[\text{M}]_{\text{eq}}}{[\text{H}]_{\text{eq}}} = \frac{x_{\text{M}}(T)}{x_{\text{H}}(T)} = \exp\left(\frac{\Delta S}{R} - \frac{\Delta H}{RT}\right) \quad (2)$$

Using eq 2 and $x_{\text{H}}(T) + x_{\text{M}}(T) = 1$ under any conditions, eq 1 can be rewritten as

$$\delta^i(T) = \frac{K(T)}{1 + K(T)}(\delta_{\text{M}}^i - \delta_{\text{H}}^i) + \delta_{\text{H}}^i \quad (3)$$

Finally, ΔH , ΔS , δ_{H}^i , and δ_{M}^i can be determined using unweighted least-squares fitting by minimizing quantity *R* as follows:⁴⁶

$$R = \sum_{i,j} (\delta^i(T_j)^{\text{calc}} - \delta^i(T_j)^{\text{expt}})^2 \quad (4)$$

where *i* and *j* are the index peaks and temperature values, respectively. Figure 7 shows the results of the nonlinear curve fitting analysis with eqs 3 and 4 using the temperature-dependent ^1H NMR spectra of TFM28H in THF-*d*₈ (see also Table S4 in the Supporting Information). The determined thermodynamic parameters of ΔH ($-12.4 \text{ kJ mol}^{-1}$) and ΔS ($-57.2 \text{ J K}^{-1} \text{ mol}^{-1}$) indicate that the proposed reaction is exothermic and spontaneous. In other words, conformer **M** is energetically more stable, which is in good agreement with the temperature-dependent absorption data.

Since the equilibrium between the two conformational isomers is quite sensitive to the solvent environment, the temperature-dependent ^1H NMR spectra of TFM28H were measured in two different solvents. The overall temperature dependence for the ^1H NMR spectra of TFM28H in toluene-*d*₈ was similar to those in THF-*d*₈ with a slightly smaller ΔH (-9.9 kJ mol^{-1}) and ΔS ($-35.5 \text{ J K}^{-1} \text{ mol}^{-1}$) (Figures S14 and S15 in the Supporting Information). Interestingly, the crossing of peak positions for the two NH protons was not experimentally observed in toluene-*d*₈ within the temperature range of 183–298 K. Moreover, the

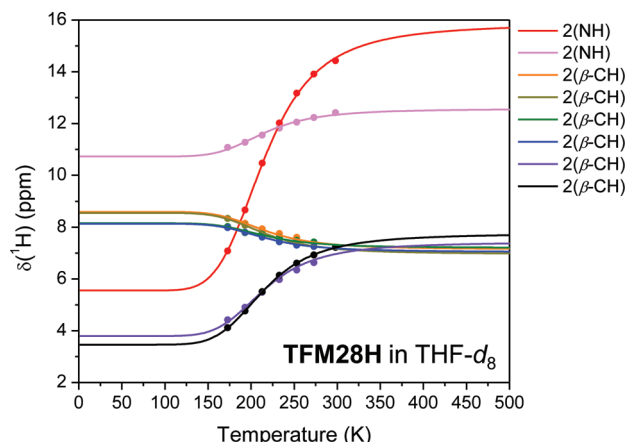


Figure 7. Experimental (closed circles) and fitted (solid lines) ^1H NMR chemical shifts of TFM28H in THF-*d*₈ as a function of temperature.

^1H NMR spectra of TFM28H in CD₂Cl₂ did not show any noticeable changes such as peak shifts with the same temperature variation, where the whole ^1H NMR spectra resembled the spectra in THF-*d*₈ at room temperature (Figure S16 in the Supporting Information). This indicates that the Hückel anti-aromatic conformer becomes dominant in CD₂Cl₂, which is also consistent with the spectral features in the absorption spectra in CH₂Cl₂ (Figures 1 and 2).

For a quantitative understanding of the solvent-dependent equilibrium dynamics, simple parameters such as critical temperature T_{unity} and crossing temperature T_{cross} were introduced. The former is defined as the specific temperature at which the same number of the two conformers exist ($K = 1$ at T_{unity}). The latter one corresponds to a crossing point between two distinct NH bands (Figure 7 and Figure S15 in the Supporting Information). According to the fitting of the ^1H NMR spectra by eqs 2 and 3, the critical temperatures were determined to be 216 and 278 K in THF-*d*₈ and toluene-*d*₈, respectively. Unfortunately, in the case of CD₂Cl₂, the determination of the critical temperature or equilibrium constant was not possible due to the fact that there were no remarkable changes in the temperature-dependent NMR spectra (Figure S16 in the Supporting Information). Because of the similarities in all of the temperature-dependent NMR spectra in CD₂Cl₂ compared with those in THF-*d*₈ at room temperature, it can be estimated that both critical temperature and crossing temperature in CD₂Cl₂ seem to be much lower than those in toluene-*d*₈ and THF-*d*₈. The temperature-dependent chemical shift changes for the most shielded NH protons and the equilibrium constants in the three solvents were plotted as shown in Figure 8.

Molecular Structures of Conformer M for TFM28H. Because of the least-squares fitting analyses of the temperature-dependent NMR spectra of TFM28H, the extrapolated chemical shifts of conformers **H** and **M** could also be determined. Because all the temperature-dependent NMR data used in the fitting analyses consisted of half the numbers of single peaks compared to the total number of protons, conformers **H** and **M** should have C₂ symmetric geometries (Table S4 in the Supporting Information). While this requirement is satisfied in conformer **H**, the optimized Möbius aromatic conformer **M** had a lower symmetric structure giving rise to complicated calculations for the ^1H NMR spectra in sharp contrast to the expected one from the temperature-dependent NMR analyses (Table 1, Figures 4, and S17 in the

Supporting Information).^{21,22} This large discrepancy suggests that dynamic interconversion between the two conformers still occurs rapidly even at 173K.

A similar dynamic equilibrium between the Möbius aromatic and Hückel antiaromatic conformers was observed in di-*p*-benzi[28]hexaphyrins with an estimated critical temperature of 330 K in CDCl₃.²⁵ In that case, it is of interest that the Möbius aromatic conformer had C₂ symmetry geometry based on both X-ray

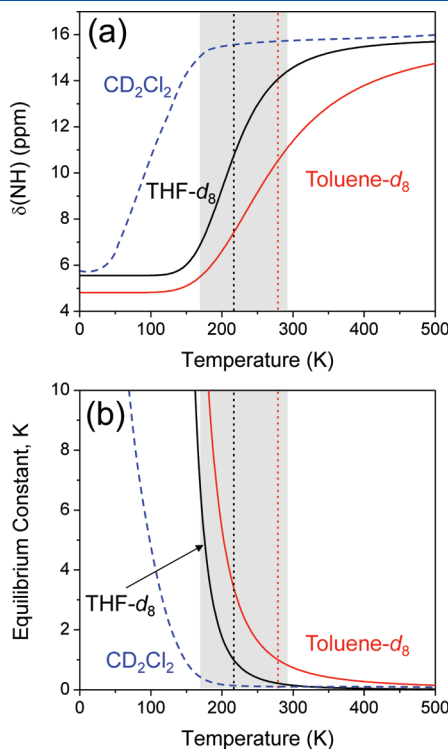


Figure 8. (a) Fitted curves of ¹H NMR chemical shifts for the most deshielded NH protons and (b) equilibrium constants of TFM28H as a function of temperature in THF-d₈ (black solid lines), toluene-d₈ (red solid lines) calculated from experimental data, and CD₂Cl₂ (estimated curves, blue dashed lines). In both figures, gray colored shaded regions correspond to our experimental temperature windows (173–298 K) and vertical dotted lines indicate the critical temperature T_{unity} of 216 K for THF-d₈ (black dots) and 278 K for toluene-d₈ (red dots), respectively.

crystallographic data and quantum mechanical calculations. Interestingly, the overall spectral changes in the ¹H NMR spectra of TFM28H in the temperature range of 173–298 K are quite similar to those of *meso*-aryl [28]hexaphyrins in 1,1,2,2-tetrachloroethane-d₂ in the temperature range of 198–413 K.²² Furthermore, the crossing temperature, T_{cross} , was determined to be ~400 K, giving rise to the estimated T_{unity} value of ~380 K, which is much higher than that of TFM28H. It should be noted that ¹H NMR peaks split and became complicated with a loss of C₂ symmetry below ~200 K. In this case, although the Möbius aromatic conformer was dominant in equilibrium at room temperature, a rapid interconversion led to the C₂ symmetry feature in the ¹H NMR spectra. Hence, in this study, we think that it is possible to observe the intrinsic ¹H NMR spectra of the Möbius aromatic conformer M at a much lower temperature than 173 K at which the solvent freezes.

According to a series of temperature-dependent NMR spectra for three kinds of [28]hexaphyrins, their equilibrium dynamics were highly dependent on the solvent as well as the temperature. The critical temperature increases in ascending order of TFM28H (216 K in THF-d₈), di-*p*-benzi[28]hexaphyrins (330 K in CDCl₃), and *meso*-aryl [28]hexaphyrin (380 K in 1,1,2,2-tetrachloroethane-d₂), indicating that the activation barrier for the interconversion processes between Hückel antiaromatic and Möbius aromatic conformers increases in the same order (Figure S18 in the Supporting Information). The authors strongly believe that a nearly barrierless activation energy for the conformational changes of TFM28H originates from the relatively more flexible figure-eight geometry induced by the sterically less-hindered trifluoromethyl substituents compared with the di-*p*-benzi[28]-hexaphyrins and *meso*-aryl [28]hexaphyrins. In a similar way, it can also be said that the activation barrier decreases as the dielectric constant increases in TFM28H based on the temperature-dependent ¹H NMR and solvent-dependent absorption spectra. In the case of di-*p*-benzi[28]hexaphyrins, the interconversion between aromatic and antiaromatic conformations can be affected by the rotation of one *p*-benzene moiety.²⁵ According to the present results, although a detailed mechanism for the interconversion could not be determined, it is postulated that a large structural change followed by bond rotation along at least two C_α–C_{meso} bonds should be compulsory for the conformational change between conformers H and M (see Figure S19 in the Supporting Information).

Table 1. Measured and Calculated Chemical Shifts in ¹H NMR Spectra of Two Conformers in TFM28H

signal	δ (conformer H) [ppm]			δ (conformer M) [ppm]		
	THF-d ₈ ^a	toluene-d ₈ ^a	GIAO ^b	THF-d ₈ ^a	toluene-d ₈ ^a	GIAO ^b
2(NH)	15.90	16.25	19.61, 19.64	5.52	4.81	−0.14, 0.17 (inner 2(NH))
2(NH)	12.58	12.86	15.34, 15.36	10.73	10.00	3.13 (NH) ^c 13.34 (NH) ^d
2(β-CH)	7.14	7.04	7.08, 7.04	8.59	7.65	7.87–9.50 (outer 8(β-CH))
2(β-CH)	6.95	6.69	5.84, 5.90	8.55	7.78	
2(β-CH)	7.19	6.57	6.95, 6.97	8.15	7.38	
2(β-CH)	7.04	6.79	6.38, 6.43	8.13	7.08	
2(β-CH)	7.44	6.97	8.77, 8.77	3.79	3.50	4.51, 5.14 (2(β-CH)) ^c
2(β-CH)	7.77	7.05	8.30, 8.35	3.46	2.80	−3.68, −4.15 (2(β-CH)) ^d

^a Intrinsic chemical shift values of the conformers H and M calculated from experimental ¹H NMR spectra based on eq 3. ^b Calculated by the GIAO method at the B3LYP/6-31G(d,p) level using the optimized geometry of each conformer. ^c Because of the protons attached from distorted pyrroles in the Möbius structures (see Figure S17 in the Supporting Information for clear assignment). ^d Because of the protons attached from inverted pyrroles in the Möbius structures (see Figure S17 in the Supporting Information for clear assignment).

CONCLUSIONS

In summary, various steady-state and time-resolved spectroscopic measurements for *meso*-trifluoromethyl substituted [26]- and [28]hexaphyrins were done along with theoretical calculations. While aromatic **TFM26H** exists as a single figure-eight conformer in solution, two conformational isomers for **TFM28H** exist in dynamic equilibrium, and their equilibrium is quite sensitive to solvent and temperature effects. In the case of **TFM28H**, it is believed that one conformer having a short S₁-state lifetime of 10 ps corresponds to the Hückel antiaromatic species with a double-sided figure-eight structure, whereas the other one should be the Möbius aromatic one with a distorted orientation in structure having a 25-fold longer S₁-state lifetime (~250 ps). Through our findings, we have demonstrated that the conformational dynamics on aromatic and antiaromatic mixtures in equilibrium can provide useful information on the structure/property relationship between aromatic and antiaromatic expanded porphyrin systems.

ASSOCIATED CONTENT

Supporting Information. Complete citations for refs 18, 21, 22, and 31; steady-state absorption and TA spectra in CH₂Cl₂; temperature-dependent ¹H NMR spectra in toluene-d₈; and CD₂Cl₂, NICS, and HOMA calculations for **TFM26H** and **TFM28H**. This material is available free of charge via the Internet at <http://pubs.acs.org>.

AUTHOR INFORMATION

Corresponding Author

*E-mail:osuka@kuchem.kyoto-u.ac.jp (A.O.); dongho@yonsei.ac.kr (D.K.).

ACKNOWLEDGMENT

This work was supported by the Midcareer Researcher Program (2010-0029668) and World Class University (R32-2010-000-10217) Programs of the Ministry of Education, Science, and Technology (MEST), Korea (to D.K.). M.C.Y. gratefully thanks the postdoctoral fellowship of the BK 21 program from the MEST, Korea. The quantum calculations were performed using the supercomputing resource of the Korea Institute of Science and Technology Information (KISTI). The work at Kyoto University was financially supported by Grants-in-Aid for Scientific Research (Nos. 22245006 (A) and 20108001 “pi-Space”) from MEXT, Japan.

REFERENCES

- Krygowski, T. M.; Cyrański, M. K. *Chem. Rev.* **2001**, *101*, 1385–1420.
- Garratt, P. J. *Aromaticity*; John Wiley & Sons: New York, 1986.
- Minkin, V. I.; Glukhovtsev, M. N.; Simkin, B. Y. *Aromaticity and Anti-aromaticity: Electronic and Structural Aspects*; John Wiley & Sons: New York, 1994.
- Ajami, D.; Oeckler, O.; Simon, A.; Herges, R. *Nature* **2003**, *426*, 819–821.
- Rappaport, S. M.; Rzepa, H. S. *J. Am. Chem. Soc.* **2008**, *130*, 7613–7619.
- Yoon, Z. S.; Osuka, A.; Kim, D. *Nat. Chem.* **2009**, *1*, 113–122.
- Herges, R. *Chem. Rev.* **2006**, *106*, 4820–4842.
- Castro, C.; Chen, Z.; Wannere, C. S.; Jiao, H.; Karney, W. L.; Mauksch, M.; Puchta, R.; van Eikema Hommes, N. J. R.; Schleyer, P. v. R. *J. Am. Chem. Soc.* **2005**, *127*, 2425–2432.
- Heilbronner, E. *Tetrahedron Lett.* **1964**, *5*, 1923–1928.
- Rzepa, H. S. *Chem. Rev.* **2005**, *105*, 3697–3715.
- Stępień, M.; Sprutta, N.; Łatos-Grażyński, L. *Angew. Chem., Int. Ed.* **2011**, *50*, 4288–4340.
- Miliordos, E. *Phys. Rev. A* **2010**, *82*, 062118–1–062118–6.
- Park, J. K.; Yoon, Z. S.; Yoon, M.-C.; Kim, K. S.; Mori, S.; Shin, J.-Y.; Osuka, A.; Kim, D. *J. Am. Chem. Soc.* **2008**, *130*, 1824–1825.
- Shin, J.-Y.; Kim, K. S.; Yoon, M.-C.; Lim, J. M.; Yoon, Z. S.; Osuka, A.; Kim, D. *Chem. Soc. Rev.* **2010**, *39*, 2751–2767.
- Lim, J. M.; Yoon, Z. S.; Shin, J.-Y.; Kim, K. S.; Yoon, M.-C.; Kim, D. *Chem. Commun.* **2008**, *261*–273.
- Yoon, M.-C.; Cho, S.; Suzuki, M.; Osuka, A.; Kim, D. *J. Am. Chem. Soc.* **2009**, *131*, 7360–7367.
- Muranaka, A.; Matsushita, O.; Yoshida, K.; Mori, S.; Suzuki, M.; Furuyama, T.; Uchiyama, M.; Osuka, A.; Kobayashi, N. *Chem.—Eur. J.* **2009**, *15*, 3744–3751.
- Yoon, Z. S.; et al. *J. Am. Chem. Soc.* **2006**, *128*, 14128–14134.
- Ahn, T. K.; Kwon, J. H.; Kim, D. Y.; Cho, D. W.; Jeong, D. H.; Kim, S. K.; Suzuki, M.; Shimizu, S.; Osuka, A.; Kim, D. *J. Am. Chem. Soc.* **2005**, *127*, 12856–12861.
- Yoon, M.-C.; Misra, R.; Yoon, Z. S.; Kim, K. S.; Lim, J. M.; Chandrashekhar, T. K.; Kim, D. *J. Phys. Chem. B* **2008**, *112*, 6900–6905.
- Kim, K. S.; et al. *J. Phys. Chem. A* **2009**, *113*, 4498–4506.
- Sankar, J.; et al. *J. Am. Chem. Soc.* **2008**, *130*, 13568–13579.
- Higashino, T.; Lim, J.; Miura, T.; Saito, S.; Shin, J. Y.; Kim, D.; Osuka, A. *Angew. Chem., Int. Ed.* **2010**, *49*, 4950–4954.
- Cho, S.; Yoon, Z. S.; Kim, K. S.; Yoon, M.-C.; Cho, D.-G.; Sessler, J. L.; Kim, D. *J. Phys. Chem. Lett.* **2010**, *1*, 895–900.
- Stępień, M.; Łatos-Grażyński, L.; Sprutta, N.; Chwalisz, P.; Szterenberg, L. *Angew. Chem., Int. Ed.* **2007**, *46*, 7869–7873.
- Stępień, M.; Szyszko, B.; Łatos-Grażyński, L. *J. Am. Chem. Soc.* **2010**, *132*, 3140–3152.
- Shimizu, S.; Aratani, N.; Osuka, A. *Chem.—Eur. J.* **2006**, *12*, 4909–4918.
- Allan, C. S. M.; Rzepa, H. S. *J. Org. Chem.* **2008**, *73*, 6615–6622.
- Rzepa, H. S. *Org. Lett.* **2008**, *10*, 949–952.
- Fliegl, H.; Sundholm, D.; Taubert, S.; Pichierri, F. *J. Phys. Chem. A* **2010**, *114*, 7153–7161.
- Frisch, M. J.; et al. *Gaussian 03*, revision C.02; Gaussian, Inc.: Wallingford, CT, 2004.
- Becke, A. D. *J. Chem. Phys.* **1993**, *98*, 5648–5652.
- Lee, C.; Yang, W.; Parr, R. G. *Phys. Rev. B* **1988**, *37*, 785–789.
- Ditchfield, R.; Hehre, W. J.; Pople, J. A. *J. Chem. Phys.* **1971**, *54*, 724–728.
- Ditchfield, R. *Mol. Phys.* **1974**, *27*, 789–807.
- Wolinski, K.; Hilton, J. F.; Pulay, P. *J. Am. Chem. Soc.* **1990**, *112*, 8251–8260.
- Bauernschmitt, R.; Ahlrichs, R. *Chem. Phys. Lett.* **1996**, *256*, 454–464.
- Onsager, L. *J. Am. Chem. Soc.* **1936**, *58*, 1486–1493.
- Schleyer, P. v. R.; Maerker, C.; Dransfeld, A.; Jiao, H.; van Eikema Hommes, N. J. R. *J. Am. Chem. Soc.* **1996**, *118*, 6317–6318.
- Chen, Z.; Wannere, C. S.; Corminboeuf, C.; Puchta, R.; Schleyer, P. v. R. *Chem. Rev.* **2005**, *105*, 3842–3888.
- Gouterman, M. In *The Porphyrins*; Dolphin, D., Ed.; Academic Press: New York, 1978; Vol. III, Part A.
- Song, H.-E.; Cissell, J. A.; Vaid, T. P.; Holten, D. *J. Phys. Chem. B* **2007**, *111*, 2138–2142.
- Mitchell, R. H. *Chem. Rev.* **2001**, *101*, 1301–1316.
- Jacobsen, N. *NMR Spectroscopy Explained: Simplified Theory, Applications and Examples for Organic Chemistry and Structural Biology*; Wiley-Interscience: New York, 2007.
- Bryant, R. G. *J. Chem. Educ.* **1983**, *60*, 933–935.
- Harris, D. C. *J. Chem. Educ.* **1998**, *75*, 119–121.